Finite Element Analysis of the Blanking and Stamping Processes of Nuclear Fuel Spacer Grids

R. O. Santos, L. P. Moreira, M. C. Cardoso

Abstract—Spacer grid assembly supporting the nuclear fuel rods is an important concern in the design of structural components of a Pressurized Water Reactor (PWR). The spacer grid is composed by springs and dimples which are formed from a strip sheet by means of blanking and stamping processes. In this paper, the blanking process and tooling parameters are evaluated by means of a 2D plane-strain finite element model in order to evaluate the punch load and quality of the sheared edges of Inconel 718 strips used for nuclear spacer grids. A 3D finite element model is also proposed to predict the tooling loads resulting from the stamping process of a preformed Inconel 718 strip and to analyse the residual stress effects upon the spring and dimple design geometries of a nuclear spacer grid.

Keywords—Blanking process, damage model, finite element modelling, Inconel 718, spacer grids, stamping process.

I. INTRODUCTION

THE spacer grids of nuclear fuel assembly are structural components with reticulated geometry that can be manufactured from Inconel 718 thin strips. The spacer grids are used to maintain adequate spacing between the fuel rods, to give stiffness for the fuel assembly, to improve the refrigerant mixing and to prevent damage during the nuclear fuel operation. Fig. 1 shows a spacer grid of a PWR in which a unit spacer grid cell is displayed in detail.
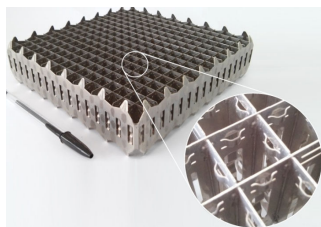

Fig. 1 Spacer grid for nuclear fuel assembly

The strips of Inconel 718, which will compose a PWR spacer grid, can be formed by a blanking process followed by a stamping process, as schematically shown in Fig. 2 in which lateral dimples and a central spring are formed the sheared workpiece.
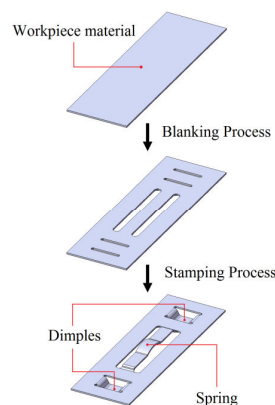
R. O. Santos is with the Graduate Program on Mechanical Engineering, Federal Fluminense University, 27255-125, Volta Redonda, Brazil (e-mail: rafaeloliveirasantos@id.uff.br).

L. P. Moreira is with the Graduate Program on Mechanical Engineering, Federal Fluminense University, 27255-125, Volta Redonda, Brazil (Phone: +55-24-2107-3730; e-mail: luciano.moreira@metal.eeimvr.uff.br).

M. C. Cardoso is with the Graduate Program on Metallurgical Engineering, Federal Fluminense University, 27255-125, Volta Redonda, Brazil (e-mail: marcelocardoso@metal.eeimvr.uff.br).

Fig. 2 The blanking and stamping process of Inconel 718 strips
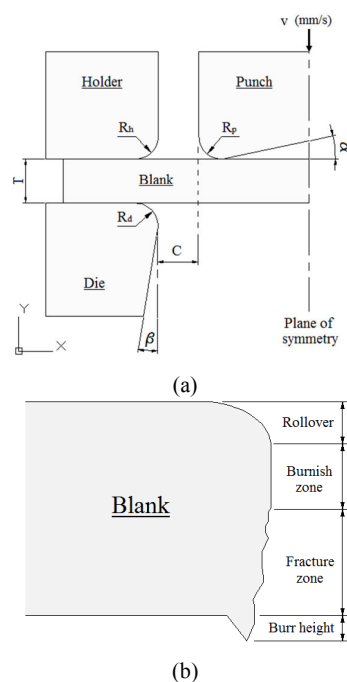

(a)

(b)

Fig. 3 Blanking process: (a) tooling parameters and (b) sheared edge

Blanking process is a shearing process, in which there are usually four characteristic regions in the cutting edge. Fig. 3 depicts a sheet blanking process wherein the workpiece material is placed between a die and a holder while it is deformed by the punch displacement. The process continues until the fracture, creating the four regions, namely, rollover, burnish zone, fracture zone and burr, as indicated in Fig. 3 (b). An ideal cutting would produce only the burnish zone without

rollover, fracture zone or undesired burr formation. However, in a real blanking process all regions are commonly observed, due to both elastic and plastic strains [1]. Besides material properties, the sheet blanking involves process parameters, such as, blanking clearance, punch velocity, sheet thickness and tooling angles [2].

In this paper, the blanking process of Inconel 718 strips used in nuclear spacer grids is firstly analysed by means of finite element simulations in order to evaluate the influence of both process and tooling parameters upon the sheared edge quality and punch load. Then, the stamping of Inconel 718 strips to form spring and dimple geometries, shown in Fig. 2, is investigated with a 3D finite element model in order to evaluate both the deformed final shape and residual stresses resulting from the forming operations.

II. MATERIAL AND METHODS

The experimentally investigated material is an Inconel 718 delivered by "*Indústrias Nucleares do Brasil (INB)*" as cold rolled thin sheet in the annealed state condition with a nominal thickness of 0.36 mm. The chemical composition of Inconel 718 provided by the supplier is listed in Table I.

TABLE I
INCONEL 718 CHEMICAL COMPOSITIONS (% WEIGHT)

Ni	Cr	Nb	Mo	Ti	Al	Fe	Cu
54.07	18.34	4.91	2.98	0.98	0.55	18.05	0.02
Si	Mn	C	Co	Ta	S	B	P
0.08	0.04	0.04	0.02	0.01	0.0005	0.003	0.006

A. Experimental Procedure

The mechanical properties of Inconel 718 sheet were evaluated by means of uniaxial tensile testing using an electromechanical universal machine 20 kN load capacity equipped with a 50 mm gauge extensometer. The specimen geometry and dimensions for uniaxial tensile testing are depicted in Fig. 4. The uniaxial tensile tests were conducted at room temperature using a constant cross-head speed of 1 mm/min. In order to ensure testing repeatability, at least three specimens were tested.
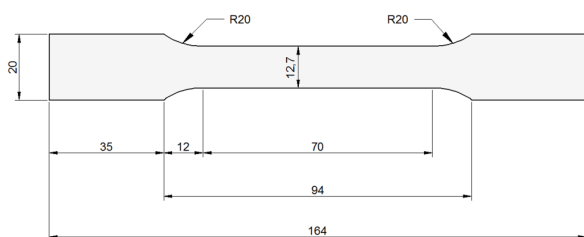

Fig. 4 Uniaxial tensile specimen dimensions (mm)

B. Damage and Fracture Modeling

A model to describe the micro-mechanical effects of damage in ductile metals is the Gurson-Tvergaard-Needleman, hereafter GTN model. Gurson first deduced a flow potential for void growth in metals assuming a perfect plastic material behaviour [3], which was later extended by Tevergaard and Needleman [4]. For a metal matrix containing a dilute concentration of voids, based on a rigid-plastic upper bound solution for spherically symmetric deformations of a single spherical void embedded in the metal matrix, Gurson proposed a yield condition of the form [5]:

$$\phi = \left(\frac{\bar{\sigma}}{\sigma_y}\right)^2 + 2\text{fcosh}\left(\frac{3}{2}\frac{\sigma_h}{\sigma_y}\right) - 1 - f^2 = 0 \qquad (1)$$

In (1), f denotes the void volume fraction in the material whereas σ_y is the yield stress of the fully dense matrix material described as a function of the effective plastic strain in the matrix and $\bar{\sigma}$ is the effective von Mises stress defined as:

$$\bar{\sigma} = \sqrt{(3/2)\boldsymbol{S} : \boldsymbol{S}} \qquad (2)$$

in which $\boldsymbol{S}$ is the deviatoric component of the Cauchy stress tensor $\boldsymbol{\sigma}$, that is, $\boldsymbol{S} = \boldsymbol{\sigma} - \sigma_h\boldsymbol{I}$ where σ_h is the hydrostatic stress component defined as $\sigma_h = (1/3)\boldsymbol{\sigma} : \boldsymbol{I}$ and $\boldsymbol{I}$ is the 2nd order identity tensor.

In the case of low stress triaxiality, Tvergaard introduced three material parameters (q_1, q_2, q_3) in (1) [4]:

$$\phi = \left(\frac{\bar{\sigma}}{\sigma_y}\right)^2 + 2q_1\text{fcosh}\left(\frac{3}{2}q_2\frac{\sigma_h}{\sigma_y}\right) - 1 - q_3f^2 = 0 \qquad (3)$$

However, the rapid loss of material stiffness is not taken into account in (3). To describe the voids coalescence affects and, therefore, to account the material stiffness changes, Tvergaard and Needleman have proposed to replace f in (1) by an effective void volume fraction f*[6]:

$$\phi = \left(\frac{\bar{\sigma}}{\sigma_y}\right)^2 + 2q_1f^*\cosh\left(\frac{3}{2}q_2\frac{\sigma_h}{\sigma_y}\right) - 1 - q_3(f^*)^2 = 0 \qquad (4)$$

with

$$f^* = \begin{cases} f & f < f_c \\ f_c + k(f - f_c) & f_c < f < f_F \end{cases} \qquad (5)$$

and

$$k = \frac{f_u^* - f_c}{f_F - f_c} \qquad (6)$$

In (6), f_c is a threshold value which indicates the onset of coalescence whereas f_F is the void volume fraction for which is verified a complete loss of material stress carrying capacity and $f_u^* = 1/q_1$ is the ultimate value of void volume fraction. In (4) σ_y stands for the current microscopic yield stress of the matrix described as a function of the corresponding effective plastic strain $\bar{\varepsilon}^p$, which according to the equivalent plastic work principle is related to the current void volume fraction f and the stress $\boldsymbol{\sigma}$ and plastic strain-rate components $\dot{\boldsymbol{\varepsilon}}^p$ as:

$$(1 - f)\sigma_y\dot{\bar{\varepsilon}}^p = \boldsymbol{\sigma} : \dot{\boldsymbol{\varepsilon}}^p \qquad (7)$$

The damage evolution in a ductile metal arises partly from growth of existing voids and partly nucleation of new voids by mechanisms of cracking or interface decohesion of inclusions

and or precipitate particles. Thus, the evolution equation for damage variable in terms of current void volume fraction rate is written as [7]:

$$\dot{f} = \dot{f}_{growth} + \dot{f}_{nucleation} \qquad (8)$$

The rate of void volume fraction growth is related to the rate of the plastic volume change as [7]:

$$\dot{f}_{growth} = (1 - f)\dot{\varepsilon}^p : I \qquad (9)$$

whereas the nucleation rate is controlled by the accumulated effective plastic strain and plastic strain-rate as:

$$\dot{f}_{nucleation} = A\, \dot{\bar{\varepsilon}}^p \qquad (10)$$

The parameter A in (10) is described by a nucleation plastic strain which follows a normal strain distribution with an average value ε_N and a corresponding standard deviation S_N [1], [5].

$$A = \frac{f_N}{S_N\sqrt{2\pi}} \exp\left[-\frac{1}{2}\left(\frac{\bar{\varepsilon}^p - \varepsilon_N}{S_N}\right)^2\right] \qquad (11)$$

in which f_N is the volume fraction of void nucleating particles. In order to describe the sheet material behaviour using GTN model one needs to specify three porous material parameters, namely, q_1, q_2 and q_3 in (4), three void nucleation parameters in (8) (ε_N, S_N and f_N), two porous failure parameters (f_c and f_F) in (5) and (6) and the initial relative density r > 0.9.

In ABAQUS FE code, the nucleation rate in (8) is not taken into account at an element integration point if the stress state is compressive, that is, voids are nucleated only when the stress triaxiality factor $\Sigma = \sigma_h/\sigma_y$ is positive [5].

In this work, the GTN model parameters were identified from finite element simulations of the experimental conditions imposed to the uniaxial tensile testing of Inconel 718 sheet. In order to simplify the numerical analysis, a single 3D solid element with only one integration point was adopted along with 1/8 symmetry displacement boundary conditions.

III. FINITE ELEMENT ANALYSIS

A. Blanking Process

The blanking is a complex process of plastic shearing and fracture in which the material at the edge become hardened locally [8]. The main process variables in sheet blanking are: (i) the punch force and velocity, (ii) the tooling material and geometry, (iii) the surface and lubrication conditions and (iv) the clearance between the punch and die.

In [9] the clearance effects on the wear blanking tooling of AISI 4340 sheet 2 mm thick were evaluated using clearances values equal to 5, 10 and 20 % of the nominal sheet thickness. For the blanking of copper, a clearance of 8 % of the sheet thickness was adopted in [8]. To analyse the shearing process of Zircaloy sheets 0.58 mm thick used in nuclear fuel spacer grids, [1] adopted clearances values of 0.01 mm and 0.02 mm. In our work, these values are adopted for the punch-die

clearance for the blanking process of Inconel 718. Moreover, values of 100 and 200 mm/min were adopted to study the influence of the punch velocity. The angle α between the punch and blank surface, indicated in Fig. 3 (a), varies in the range of 0 and 12 degrees whereas the angle β at the die wall varies between 0 and 3 degrees [10]. Therefore, assuming the tooling radii equal to 0.01 mm, see Fig. 3 (a), along with the selected punch-die clearances C-values (0.01 and 0.02 mm), the punch velocities (100 and 200 mm/min) and the different tooling angles, provided total of 16 combinations as listed in Table II.

A 2D plane-strain model was built to simulate the blanking process of Inconel 718 strips. The elastic behaviour of the blank is defined by Hooke's law with Young modulus E and Poisson's ratio v equal to 197,689 MPa and 0.29, respectively. The material plastic behaviour is defined in a tabulated form as a function of the plastic strain together with GTN model parameters. Isotropic work-hardening and associated flow rule are adopted with von Mises yield criterion.

The blanking tools were assumed as rigid and described by means of analytical rigid surfaces. Coulomb law was assumed between the tooling and blank contact surfaces with a friction coefficient equal to 0.3.

TABLE II
FE SIMULATIONS OF INCONEL 718 BLANKING PROCESS PARAMETERS

Case Number	v (mm/min)		C (µm)		α (degrees)		β (degrees)	
	100	200	10	20	0	12	0	3
11000	•		•		•		•	
12000	•			•	•		•	
11120	•		•			•	•	
12120	•			•		•	•	
11003	•		•		•			•
12003	•			•	•			•
11123	•		•			•		•
12123	•			•		•		•
21000		•	•		•		•	
22000		•		•	•		•	
21120		•	•			•	•	
22120		•		•		•	•	
21003		•	•		•			•
22003		•		•	•			•
21123		•	•			•		•
22123		•		•		•		•

Fig. 5 shows the finite element mesh built to represent the strip region of interest refined by a structured mesh [11]. The smallest element size is equal to 1.2 micrometres whereas the largest element size is equal to 48 micrometres. To avoid excessively element distortion, Arbitrary Lagrangian-Eulerian (ALE) adaptive mesh refinement is activated. The numerical simulations of Inconel 718 blanking process were performed with ABAQUS/Explicit academic research version 6.9-1 in a dual-processor Intel Xeon X5690 workstation with 3.47 GHz, 24 cores and 16 Gb RAM.
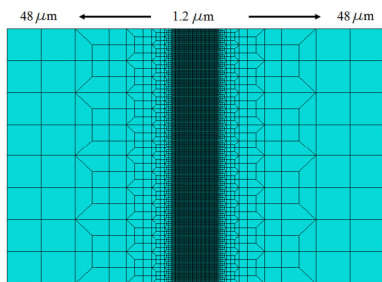
Fig. 5 FE mesh of Inconel 718 strip blanking process

B. Stamping Process

The stamping process to form both spring and dimples of the PWR spacer grid was performed in four simulation steps, schematically shown in Fig. 6. The first simulation step consisted of forming the previously assumed sheared strip in order to obtain the desired dimple shape. In the second step, the preformed strip is firstly held between the top and bottom dies and, then, the punch moves up to form the spring profile. The third step is carried out to remove the contact surfaces between the workpiece and forming tools whereas the fourth step is performed to analyse the workpiece springback.
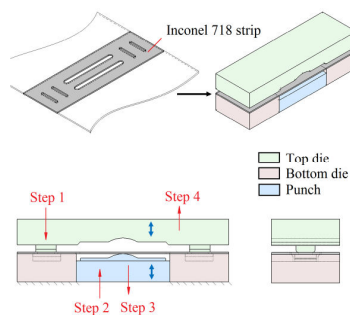
Fig. 6 FE Simulation steps of the stamping process

The total time required to achieve the Inconel 718 strip stamping process is equal to 2 seconds. Fig. 7 shows the vertical displacements prescribed to each tool during the four simulation steps. To avoid numerical instabilities arising from dynamic vibrational modes, the stamping process simulation was performed with the static implicit technique available in ABAQUS/Standard FE code. However, the available GTN model in the ABAQUS/Standard has no porous failure criteria [5]. Thus, the strip mechanical properties adopted in the 3D stamping are the same used in the 2D plane-strain blanking process except for the porous failure criteria. The stamping tools are defined by means of discrete rigid surfaces. Besides, a 1/4 symmetry 3D FE model was adopted to simplify the analysis and to save CPU time.

The strip is meshed with 46,180 linear hexahedral elements with reduced integration, C3D8R according to ABAQUS FE code terminology. Fig. 8 shows the FE meshes for the strip and the stamping tools. Fig. 8 (a) details the refined mesh in regions which are expected to achieve higher straining levels due to bending and stretching of the dimples and spring. The tooling is represented by 4-node linear quadrilateral rigid

surface R3D4 element type according to the finite element meshes shown in Figs. 8 (b)-(d) for the top-die, punch and bottom-die with 832, 332 and 454 elements, respectively. A Coulomb friction coefficient equal to 0.2 was assumed in all strip-tooling contact surfaces.
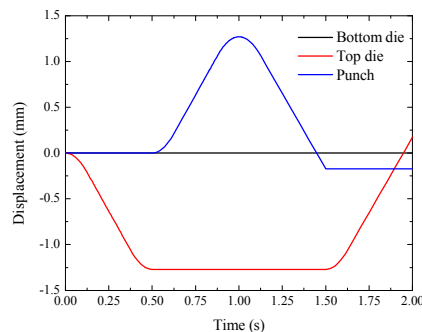

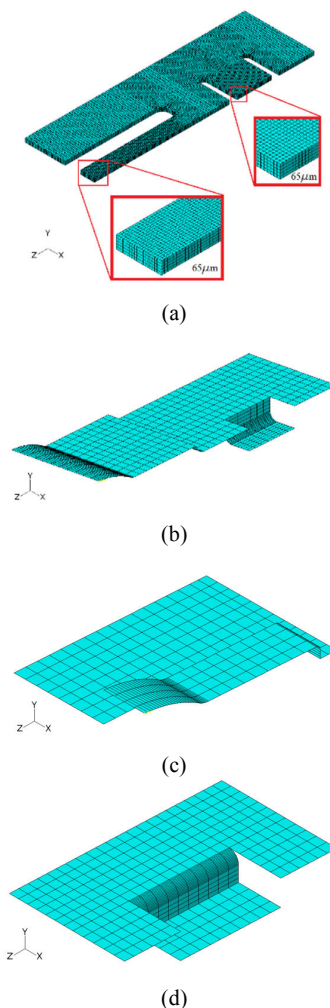Fig. 7 Kinematics of Inconel 718 stamping process FE simulation

(a)

(b)

(c)

(d)

Fig. 8 FE meshes for Inconel 718 0.36 mm strip stamping process: (a) preformed strip, (b) top die, (c) punch and (d) bottom die

IV. RESULTS AND DISCUSSION

A. Mechanical Properties

From the uniaxial tensile testing results performed at room temperature conditions under a cross-head speed of 1 mm/min, which corresponds to a nominal strain-rate about 3×10^{-4} s^{-1}. The obtained engineering stress-strain curve, shown in Fig. 9, provided similar mechanical behaviour with the experimental values of Inconel 718 1.6 mm thick sheets investigated in [12]. Inconel 718 strip 0.36 mm thick presented a good ductility along with a high work-hardening rate. However, Inconel 718 0.36 mm thick sheet showed an abrupt fracture without any apparent localized necking, as indicated in Fig. 10 (b).
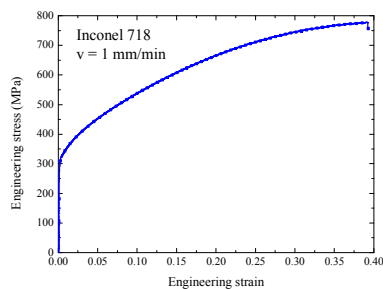
Fig. 9 Inconel 718 0.36 mm sheet experimental uniaxial tensile engineering stress-strain curve
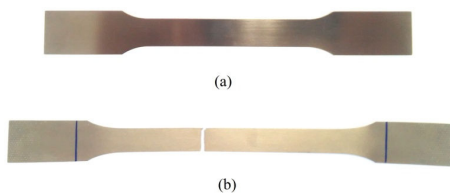

Fig. 10 Inconel 718 0.36 mm thick sheet uniaxial tensile specimens: (a) unreformed and (b) fractured conditions

B. Identification of GTN Model Parameters

According to the literature [1], [5], the recommended values of GTN yield function parameters (q_1, q_2 and q_3) to describe the ductile fracture of metals are: $q_1 = 1 - 1.5$, $q_2 = 1$ and $q_3 = q_1^2 = 1 - 2.25$. The calibration of all nine GTN material parameters was performed from FE simulations of a single 3D solid element with 1/8 symmetry displacement boundary conditions. Table III lists the best fit parameters set which were obtained in comparison to the experimental true stress-strain uniaxial tensile of Inconel 718 0.36 mm thick sheet. Fig. 11 compares the numerical predicted uniaxial true stress-strain curve calculated from the GTN model parameters with the Inconel 718 experimental data.

TABLE III
GTN MODEL PARAMETERS FOR INCONEL 718 0.36 MM SHEET

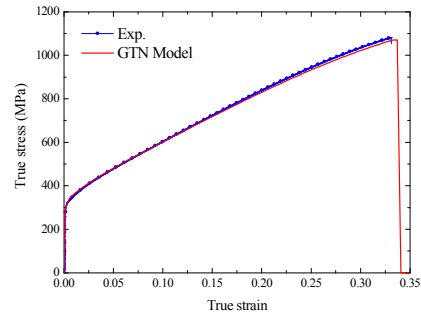| r	q_1	q_2	q_3	ε_N	S_N	f_N	f_F	f_C
0.999	1.2	1	1.44	0.1	0.05	0.005	0.008	0.00742

Fig. 11 Experimental and predicted uniaxial true stress-strain curves determined for Inconel 718 0.36 mm sheet

C. Analysis of Blanking Process and Tooling Parameters

Fig. 12 shows the predicted blanking punch force as a function of the normalized displacement with respect to initial blank thickness. These predictions were determined from 16 combinations defined in Table II. For discussion purposes, four data sets were proposed according to the simulated cases. The first one, is composed by all numerical results obtained for the punch velocity equal to 100 mm/min with the same punch rake angle ($\alpha = 0$ degrees). A similar procedure was adopted for the other sets, namely, the punch velocity and rake angle are kept constant while varying the punch-die clearance ($C = 0.01$ and 0.02 mm) and β angle (0 and 3 degrees) values. Firstly, it is worth to observe that the punch force decreases with an increase of the angle α between the punch and blank surface, which is directly related to the contact area decrease. Secondly, cases for which β angle die is equal to 3 degrees, the punch force decreases faster after attaining a maximum, than in the cases where β angle was set equal to zero degrees. In addition, the normalized punch displacement forces indicate that the blanking process is completed between ~ 40 and 45 % of the initial Inconel 718 blank thickness.

Table IV summarizes the numerical predictions determined from the 16 process and tooling parameters combinations defined in Table II in terms of the percent values of burnish, rollover and fracture zones together with burr height (micrometres) and the maximum punch load, respectively. Bearing in mind an ideal blanking process free of any cutting defects, the adopted quality criterion of the sheared edge is based upon the largest burnish area. Thus, the simulated cases in Table IV are ranked from the best process and tooling parameters set defined by v = 100 mm/ min, C = 0.01 mm, $\alpha = 12$ degrees and $\beta = 3$ degrees, up to the worst parameters set given by v = 100 mm/min, C = 0.02 mm, $\alpha = 0$ degrees and $\beta = 3$ degrees. Fig. 13 shows the corresponding predicted sheared edge profiles obtained from cases (11123 and 12003). It is worth to observe the deformed blank mesh indicating the cutting zones. Actually, the sheared edge predictions are highly affected by the region mesh density as well as the element deletion procedure mainly near to the burr zone formation where the elements become too distorted.
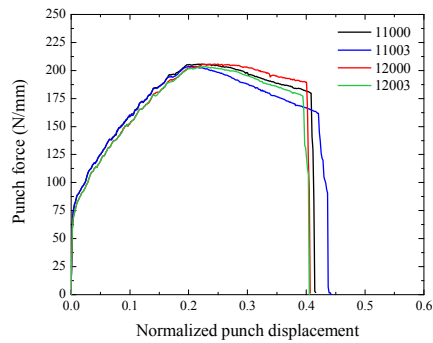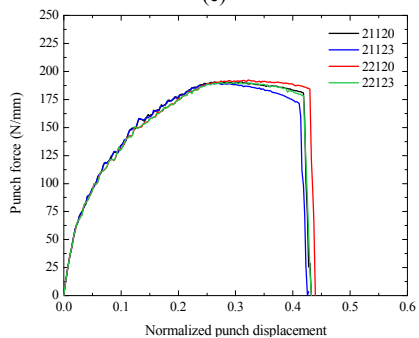
(a)
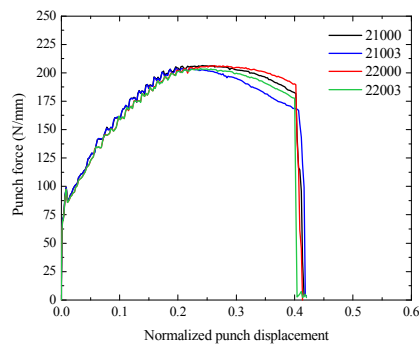
(b)
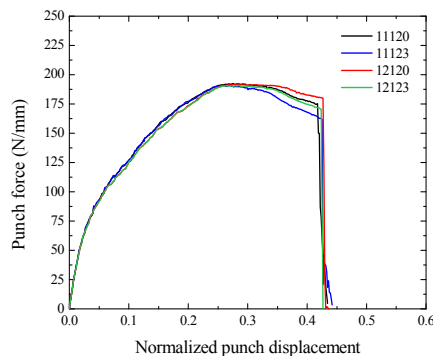
(c)

Fig. 12 Predicted punch force determined for the blanking process of Inconel 718 0.36 mm strip: (a) v = 100 mm/min and α = 0 degrees, (b) v = 200 mm/min and α = 0 degrees, (c) v = 100 mm/min and α = 12 degrees, (d) v = 200 mm/min and α = 12 degrees

TABLE IV
RANKING FROM THE PROPOSED NUMERICAL SIMULATIONS FOR THE
BLANKING PROCESS OF INCONEL 718 STRIP

Ranking	Case number	Burnish (%)	Rollover (%)	Fracture (%)	Burr (μm)	Load (N/mm)
1st	11123	30.1	12.5	57.4	5.41	190.5
2nd	21120	29.3	12.3	58.4	2.57	190.2
3rd	21123	28.7	12.1	59.3	3.80	189.6
4th	12123	28.6	13.0	58.4	2.06	190.5
5th	11003	28.0	13.4	58.6	6.63	203.8
6th	11120	28.0	12.7	59.4	3.74	192.8
7th	21003	27.6	13.2	59.2	6.98	204.1
8th	21000	27.5	13.1	59.4	6.08	206.5
9th	22123	27.3	13.6	59.1	2.11	190.1
10th	22120	27.0	12.6	60.3	3.09	192.3
11th	11000	26.5	14.4	59.1	3.91	205.6
12th	12120	26.4	14.1	59.5	4.61	191.8
13th	12000	26.3	13.4	60.3	7.68	205.7
14th	22000	25.2	14.8	60.0	2.17	206.3
15th	22003	24.8	14.6	60.6	3.71	203.7
16th	12003	24.1	13.9	62.0	2.38	203.3
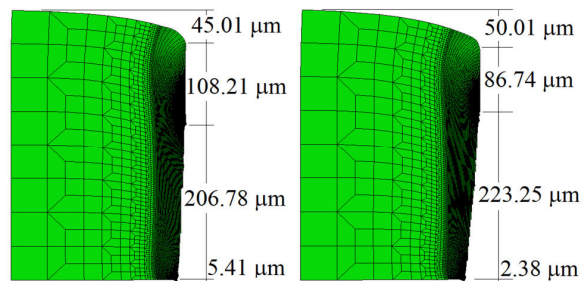
(a) 11123   (b) 12003

Fig. 13 Sheared edge profiles predicted by FE simulations of the blanking process of Inconel 718 strips: (a) 11123 and (b) 12003 cases defined by the process and tooling parameters listed in Table II

Fig. 14 shows the predicted contour plots of the void volume fractions obtained from the best process and tooling parameters set (case 11123) at an instant time before the workpiece fracture. From the total void volume fraction, shown in Fig. 14 (a), it can be observed that the regions under compression present small values of the void volume fraction. The zones in which the burnish and fracture occur, Fig. 14 (b), displayed larger void growth whereas the process nucleation of new voids takes place in the rollover zone, see Fig. 14 (c). The void volume fraction due to the nucleation determined from the case 11003 is shown in Fig. 15. This specific case has the same tooling parameters of the best configuration set except for the punch rake angle which is equal to 0 degrees. Considering the same time instant prior of the blank fracture, the punch with zero rake angle will produce a higher volume fraction of voids due the faster nucleation rate in the rollover zone than a punch geometry with a rake angle of 12 degrees. Consequently, Inconel 718 strips sheared by a punch with no rake angle will result in larger rollover areas.
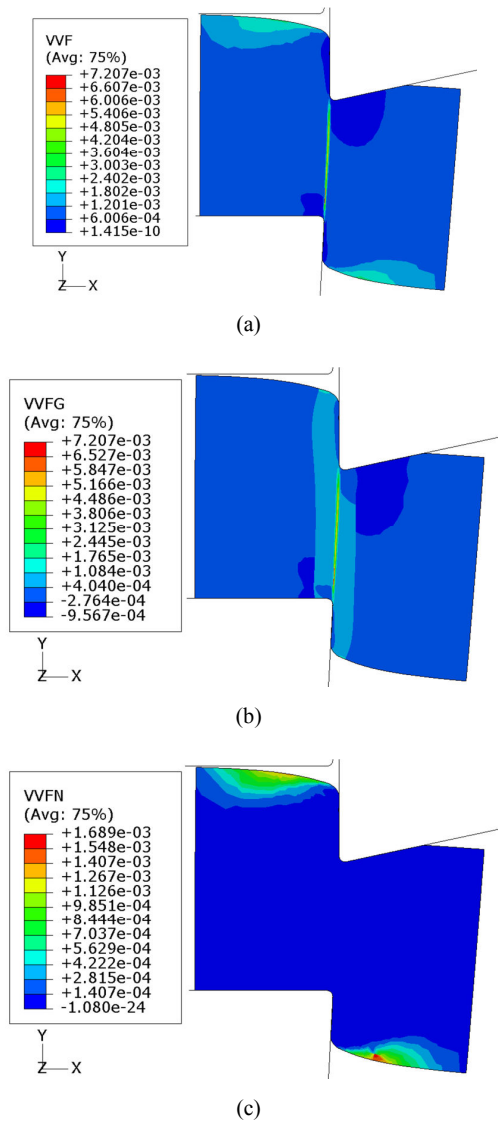
(a)

(b)

(c)

Fig. 14 Predicted void volume fractions obtained from 11123 case:
(a) total void volume fraction (VVF), (b) void growth volume
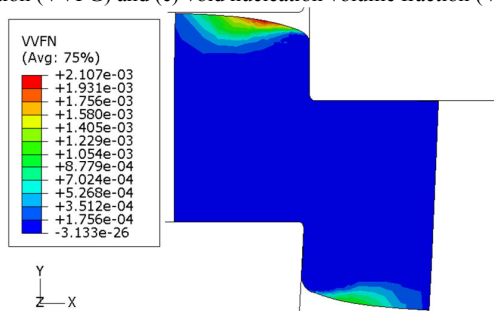fraction (VVFG) and (c) void nucleation volume fraction (VVFN)

Fig. 15 Case 11003 void nucleation volume fraction (VVFN)

D. Analysis of the Stamping Process

The FE simulation of the preformed Inconel 718 stamping process was completed in four steps. The predicted tooling forces are shown in Fig. 16 as a function of the process time.

In the first step, the top-die needs an amount of ~ 2,860 N to form the dimples. Secondly, the punch displaces upwards, while the work piece is held between both top and bottom dies, to form the spring to reach a maximum reaction of ~ 1,880 N. Afterwards, the reaction forces drops to zero due to the tools displacements back to their original positions.
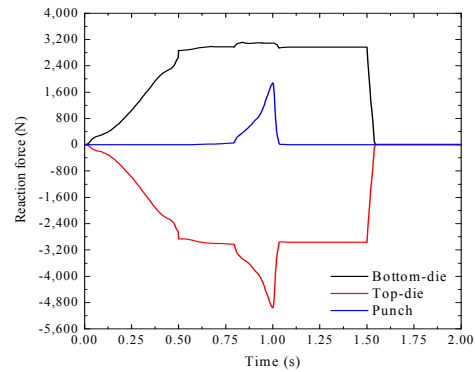

Fig. 16 Predicted tooling forces from the stamping process

Fig. 17 shows the deformed mesh geometry obtained from the finite element simulation of Inconel 718 stamping process. In this figure are indicated both longitudinal and transverse directions along the symmetry planes YZ and XY, respectively. Springback effects are expected after removing the work piece from the tooling. In order to evaluate these undesired effects, the designed profile geometries of both spring and dimples outside surfaces are compared in Fig. 18 to the numerical predictions obtained after releasing the tooling. The spring and dimple profiles were obtained along the longitudinal and transverse distances defined from XY and YZ symmetry planes, respectively. The spring moves back about 0.112 mm whereas the dimple springs back about 0.026 mm. Fig. 19 shows the residual stresses contour plots (in 10^9 Pa) determined along the X, Y and Z Cartesian axes coordinates. The most important residual stress levels are tensile along the Z-direction; see Fig. 19 (c), located near to the smaller spring radius and close to the outer surface of the dimple bending.
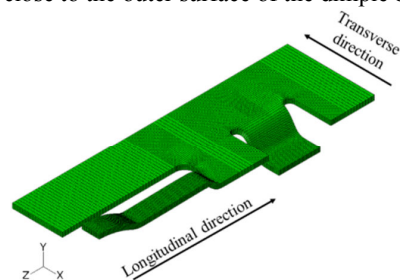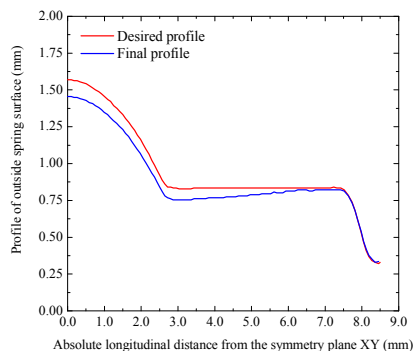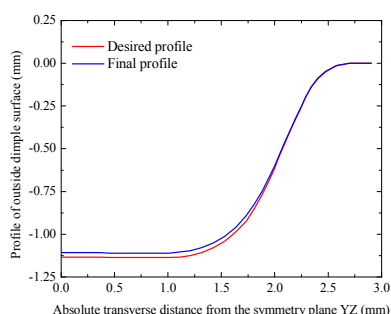

Fig. 17 Predicted deformed geometry from the stamping process

(a)

(b)

Fig. 18 Predicted profile outside surfaces after removing the tooling:
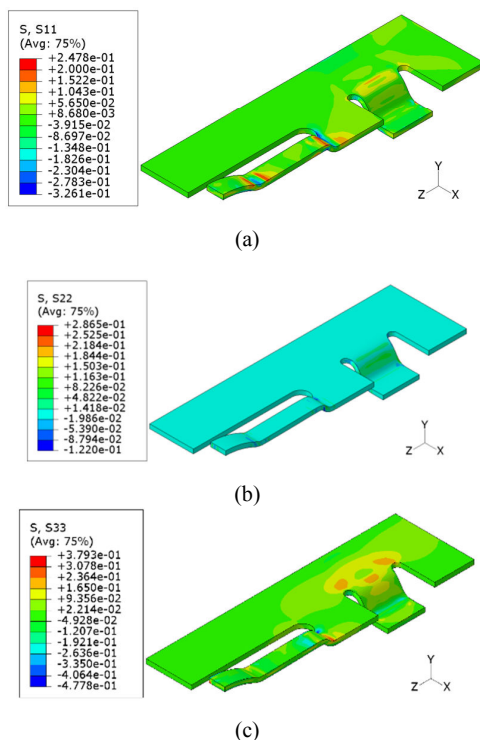(a) spring and (b) dimple

(a)

(b)

(c)

Fig. 19 Residual stress distributions obtained after tooling removal:
(a) X-direction (S11), (b) Y-direction (S22) and Z-direction (S33)

V. CONCLUSION

In this work, the mechanical properties of Inconel 718 strip 0.36 thick were evaluated by means of uniaxial tensile tests in order to fit GTN model parameters. The obtained set of damage parameters allowed defining an element removal technique in the ABAQUS/Explicit FE code to simulate the blanking process of Inconel 718 strip. A set of 16 numerical simulations was performed to forecast the sheared edge zones and the shearing punch load. From the numerical predictions, the optimum blanking process and tooling parameters set is defined by punch velocity v = 100 mm/min, die-punch tooling clearance C = 0.01 mm, punch rake angle α = 12 degrees and die wall angle β = 3 degrees. This set provided 30.1% of burnish, 12.5% of rollover, 57.4% of fracture zones together with a burr height of 5.41 micrometres. The maximum punch force was of 190.5 N per length unit. It was observed that the punch rake angle has an important influence upon the shearing load and the rollover zone formation. From the GTN damage results, the voids are formed mainly in the fracture and rollover zones. The void volume fraction due the growth is more important within the fracture zone whereas the void volume fraction due the nucleation is predominant in the rollover area. However, both the mesh density and adopted element removal technique must be further investigated in order to better predict the burr formation.

The stamping process assuming a preformed Inconel 718 strip was successfully simulated with the proposed four step process to form both spring and dimple geometries of nuclear spacer grids. The finite element predictions of this stamping process allowed evaluating the required tooling forces. Also, residual stress effects arising from the tooling removal caused minor geometry changes in both spring and dimple outer designed surface profiles.

REFERENCES

[1] J. Wang, N. Kim, and H. Lee, "Ductile fracture in the shearing process of Zircaloy sheet for nuclear fuel spacer grids". In *Metal and Materials International*, vol. 18, No. 2, 2012, pp. 303-316.
[2] C. Poizat, L. Champagne, L. Daridon, L. Ahzi, C. Husson, and L. Merle, "Modeling and simulation of thin sheet blanking using damage and rupture criteria". In International Journal of Forming Process, vol. 8, No.1, 2005, pp.29-47.
[3] A. L. Gurson, "Continuum theory of ductile rupture by void nucleation and growth. I. Yield criteria and flow rules for porous ductile media". In *Journal of Engineering Materials and Technology*. vol. 99, No. 1, 1977, pp. 2-15.
[4] A. Needleman and V. Tvergaard, "An analysis of ductile rupture in notched bars". In *Journal of the Mechanics and Physics of Solids*. vol. 32, No 6, 1984, pp. 461-490.
[5] ABAQUS user's manual, Version 6.9, Dassault Systemes Simulia Corp., Providence, RI, USA, 2009.

[6] A. Slimane, B. Bouchouicha, M. Benguediab and S. A. Slimane, "Parametric study of the ductile dameage by the Gurson-Tvergaard-Needleman model of structures in carbon steel A48-AP". In *Journal of Materials Research and Technology*, vol. 4, No. 2, 2015, pp. 217-223.

[7] C. C. Chu and A. Needleman, "Void nucleation effects in biaxially stretched sheets". In *Journal of Engineering Materials and Technology*. vol. 102, 1980, pp. 249-256.

[8] J. Marciniak, J. L. Ducan and S. J. Hu, *Mechanics of sheet metal forming*, 2nd Ed, London, 2002.

[9] D. C. Ko and B. M. Kim, "Development of an analytical scheme to predict the need for tool regrinding in shearing process". In *International of Machine Tools & Manufactur*e, vol. 40, 2000, pp. 1329-1349.

[10] V. Boljanovic, *Sheet metal forming process and die design*, Industrial Press, New York, 2004.

[11] B. B. Anjos and L. P. Moreira, "Experimental and numerical analysis of the lateral cutting of hot rolled strips steel". In *VIII Congresso Nacional de Engenharia Mecânica*, Uberlândia, Brasil, 2014.

[12] N. D. Alexopoulos, N. Argyriou, V. Stergiou and S. K. Kourkoulis, "Fatigue behavior of Inconel 718 TIG welds". In *Journal of Materials Engineering and Performance*. vol. 23, 2014, pp. 2973-2983.

R. O. Santos was born in Barra Mansa, Rio de Janeiro state, Brazil, 1988. He graduated from Mechanical Engineering at Federal Fluminense University, Volta Redonda, in 2013. Now, he is a Master student at the same university with a scholarship from CAPES/Eletronuclear program. His dissertation subject is about the shearing and stamping processes of nuclear spacer grids.

L. P. Moreira received his 'Docteur en Sciences' in Mechanics of Materials from Metz University in 2002. He is currently Associate Professor at the Department of Mechanical Engineering, Federal Fluminense University, Volta Redonda, Rio de Janeiro, Brazil. His research interests include the modelling and simulation of metal forming processes.

M. C. Cardoso was born in Niterói, Rio de Janeiro state, Brazil, 1972. He graduated from Civil Engineering at Veiga de Almeida University, Rio de Janeiro, in 1990. He received the title of Master of Sciences in Metallurgical Engineering in 2012 at Federal Fluminense University, Volta Redonda, Rio de Janeiro state, Brazil. Now, he is a PhD. student at the same university with a scholarship from CAPES foundation. His thesis subject is about the plastic behaviour of advanced high strength steels.